Supporting Information for

Using Flow to Switch the Valency of Bacterial Capture on Engineered Surfaces containing Immobilized Nanoparticles

Bing Fang,[1] Saugata Gon,[2] Myoung Park,[3] Kushi-Nidhi Kumar,[4] Vincent M. Rotello,[3] Klaus Nüsslein,[4] and Maria M. Santore*,[1]

[1]Department of Polymer Science and Engineering
[2]Department of Chemical Engineering
[3]Deparmtent of Chemistry
[4]Department of Microbiology

University of Massachusetts
Amherst, MA 01003

Transport-limited Bacterial Capture on a Substantially Cationic Surface.

Measurement of bacterial capture efficiencies on nanoparticle-containing surfaces required measurement of transport-limited bacterial capture rates. The transport limited rates varied from batch to bacterial batch due to their proportionality to bacterial concentration, which also varied among the bacterial batches. Therefore, independent measurement of the transport-limited rate for each batch allowed the capture kinetics of the different batches to be compared, via the capture efficiency.

To measure the transport-limited capture rates, a substantially adhesive surface was needed. For this purpose, an adsorbed layer of poly-l-lysine (PLL) was chosen. Capture of negatively-charged *S. Aureus* (ζ = -12, -25, and -24 mV at ionic strengths corresponding to κ^{-1} = 1, 2, and 4 nm, respectively) on cationic PLL was expected to be transport-limited, due to the lack of an energy barrier opposing capture. Figure A1 examines the adhesion of *S. Aureus* on PLL layers. In part A, typical raw data are shown: At low wall shear rates, bacterial accumulation is mostly linear in time, especially within the first few minutes. At higher wall shear rates the initial bacterial capture rate is generally greater, but the turnover after the first few minutes is more pronounced. In all cases, however, the initial slopes of the raw data are well-defined. These initial slopes, which provide insight into the bacteria-surface interactions (as opposed to bacteria-bacteria interactions), are plotted as a function of shear rate to the 1/3 power in Figure A1B. Notably, these initial rates are insensitive to ionic strength.
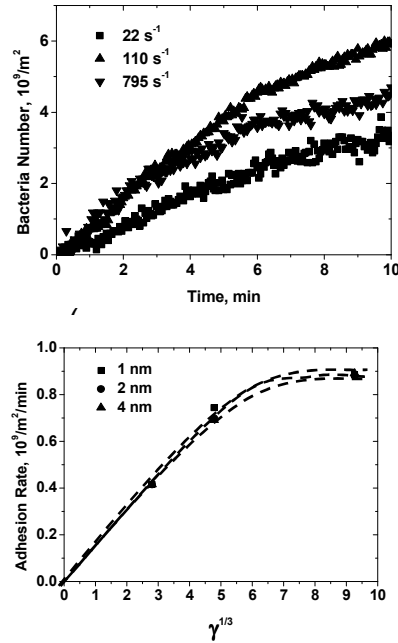
Figure A1. (A) Raw data for the capture of *S. aureus* on PLL surfaces (0.4 mg/m^2, ζ = 6 mV) in pH 7.4 phosphate buffer (I = 0.026 M and κ^{-1} = 2 nm) at wall shear rates of 22 s^{-1}, 110 s^{-1} and 795 s^{-1}. **(B)** Summary of initial *S. aureus* capture rates for different ionic strengths corresponding to κ^{-1} = 1, 2 and 4 nm, with the shear scaling motivated by the Leveque equation.

The 1/3-power law scaling of Figure A1B is motivated by the Leveque equation which predicts the pseudo-steady state transport-limited capture rate, dΓ/dt of an adsorbing species on the wall of a slit-flow chamber.[1]

$$\frac{d\Gamma}{dt} = \frac{1}{\Gamma\left(\frac{4}{3}\right)9^{\frac{1}{3}}} \left(\frac{\gamma}{DL}\right)^{\frac{1}{3}} DC \tag{1}$$

Here, C is the bacterial concentration in solution, D is its free solution diffusion coefficient, γ is the wall shear rate, L is the distance from the entrance of the flow chamber to the point of observation, and here and only here on the right side of equation 1, Γ is the gamma function. The pseudo-steady state condition is that when the concentration gradient of bacterial near the wall is fixed in time, giving rise to a fixed rate of bacterial accumulation on the surface. This occurs when the convection of bacteria to position L is matched with the diffusion of bacterial across the boundary layer at that position, so that there is no concentration change (with respect to time) in the fluid near the surface. The pseudo-steady state condition fails initially when the concentration gradient is being set up, and also near surface saturation, when the gradient dissipates. It holds for substantial periods of time when adsorption / capture is occurring and the surface is not saturated.

In Figure A1B, at low wall shear rates, the bacterial capture is linear and extrapolates to the origin. Above about 110 s^{-1}, the bacterial capture *rate* turns over. This indicates that at high shear, the hydrodynamic forces exceed those from the surface, or at least, given the complexities of the bacterial surface, the shear rate (and bacterial motion) is faster than the effective capture rate on the surface. With the goal of using PLL surfaces to facilitate a calibration of different bacterial concentrations, Figure A1B suggests this approach is valid at $\gamma = 110$s^{-1} or below, but cannot be applied at 795 s^{-1}.

The significance of the bacterial capture kinetics is put into perspective in Figure A2 by parallel studies of the capture of 1 um diameter silica spheres on the same PLL surface. The silica spheres are credible models for *S. Aureus* capture (perhaps not universally, but here for the particular issue addressed they are quite reasonable) because both the particles and the bacteria are 1 um spheres and both have negative
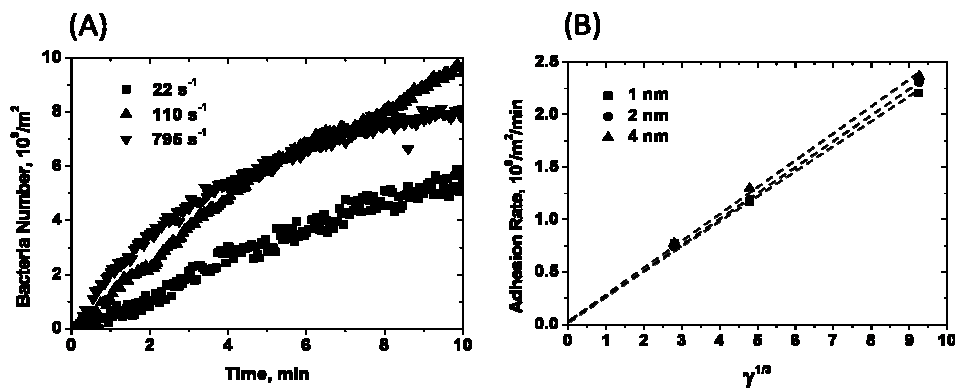

Figure A2. **(A)** Raw data for the capture of silica particles on PLL surfaces (0.4 mg/m^2, $\zeta = 6$ mV) in pH 7.4 phosphate buffer (I = 0.026 M and κ^{-1} = 2 nm) at wall shear rates of 22 s^{-1}, 110 s^{-1} and 795 s^{-1}. **(B)** Summary of initial silica particle capture rates at ionic strengths corresponding to different Debye lengths (1, 2 and 4 nm). The wall shear rate scaling is motivated by the Leveque equation.

charge, making them strongly attractive to the PLL surface. In Figure A2, the initial rates of silica microparticle capture adhere *quantitatively* to the Leveque equation for transport-limited particle capture, for the known particle concentration of 0.1 wt% and the flow chamber geometry. The 1/3-power law scaling is excellent and also without significant ionic strength dependence.

From the comparison of the initial capture rates of the bacteria and the silica one concludes that the bacterial capture rate at $\gamma = 22$ and 110 s^{-1} was indeed transport limited. While the numbers of bacteria actually captured fall modestly below those of the silica spheres, for similar nominal bacterial and particle concentrations, the bacterial concentration is not accessible with sufficient precision. The relative quantitative closeness of the two experiments reflects error in the actual bacterial concentration rather than its adsorption kinetics. The results also demonstrate real deviation from transport-limited bacterial capture kinetics at $\gamma = 795$ s^{-1}. The reasons are unclear and may involve the heterogeneities or structural details of the bacterial membrane itself. The underlying point, however, is that the measured initial bacterial adhesion rate onto PLL at $\gamma = 795$ s^{-1} is no longer an appropriate normalization factor for the main study of bacterial adhesion on nanoparticle-containing surfaces. Instead for consistency, the extrapolated transport-limited bacterial capture was used in calculations of bacterial capture efficiency.

The current paper focuses on the initial bacterial capture rates. We note, however, that the interesting curvature in the raw bacterial capture data (Figure A1A) parallel the turnover in the raw data seen for silica spheres in Figure A2A. This turnover is a result of the filling of the surface with bacteria (or microspheres), and occurs at the roughly the same coverage levels for bacteria and silica spheres, arguing for a single surface filling mechanism for the two systems. The turnover at relatively low coverage levels (less than 1 area-%) argues that this behavior is a long-range hydrodynamic effect between captured and approaching spheres, as is established in the literature.[2-4] Particles or cells already adhering to the surface hydrodynamically block the capture of further particles / cells for many tens of microns downstream of each immobilized particle. This blocking length increases with the flow rate. Our initial quantitative analysis of the spatial arrangement of captured particles and bacteria confirm this mechanism. As filling of the surface is beyond the scope of this paper, nothing more will be discussed on this topic here.

In summary, the line of Figure A1B shows an example of the transport-limited bacterial capture rates as a function of flow rate, for this particular batch of bacteria. Measuring a few such data points with each new bacterial batch (with a potentially different bacterial concentration) re-establishes the rate and enables bacterial capture rates to be compared as capture efficiencies. The transport-limited capture rate is independent of ionic strength for the Deybe length range $\kappa^{-1} = 1\text{-}4$ nm.

Statistical Model for Bacterial Capture

A statistical model, developed previously for the interpretation of silica particle capture,[5] is implemented here to assess the interfacial conditions for bacterial capture and the structure of the bacteria-surface contact zone. Key quantities addressed are the area of the initial bacteria-surface interaction (here in the supporting information) and the minimum number of nanoparticles needed for bacterial capture (in the main paper).

The model inputs a bacterial-surface interaction area, A, which is user-specified and is ultimately fit to match experimental data. Also to be specified is the critical number of nanoparticle needed to engage each bacterium during capture. This additional parameter is systematically decoupled from the fitting of the interaction area, as described below. The critical number of nanoparticles needed for bacterial capture, divided by the interaction area, is typically greater than the average nanoparticle loading (per area) on the x-axis of plots such as Figure 3. In this way, bacteria adhere only on surface regions having sufficiently above-average nanoparticle density, with the probability of their capture related to the probability of bacteria encountering theses "hot spots".

The experimentally-confirmed random distribution of the nanoparticles[6] is described here by a Poisson distribution, where P is the probability of finding an exact number, n, of nanoparticles in the interaction zone, given that N is the average number of nanoparticles in the interaction area.

$$P_N(n) = \frac{N^n e^{-N}}{n!}$$
(A1)

The average concentration, N/A, of nanoparticles in the interaction zone is the same as the average surface loading on the x-axis of Figure 3. Therefore specification of A allows determination of N along the x-axis of Figure 3.

Capture occurs when approaching bacteria encounter a number of nanoparticles that exceeds some critical number, n_{crit}, in the interaction area. The Poisson distribution is therefore summed above this critical number to yield the complement of the cumulative distribution function, $P_A(N)$.

$$P_A(N) = \sum_{n=n_{crit}}^{\infty} P_N(n) \tag{2}$$

$P_A(N)$ describes the probability of bacterial capture, as a function of the average number, N, of nanoparticles in the interaction area. Again this latter quantity is proportional to the x-axis of Figure 3.

The probability of capture is proportional to the observed bacterial capture rate, in the regime where bacterial capture is surface-limited. When this probability becomes large, the intrinsic bacterial capture rate becomes too fast to be experimentally measured and, instead, the transport-limited capture rate is observed. While a precise treatment uses the surface-limited rate as a boundary-condition for the transport problem, a reasonable approximation for surface-controlled bacterial capture like that in the current study, is to simply assign a transport-limited maximum above which high capture probabilities cannot be measured. This approach is shown in the next section.

Monovalent Capture and the Initial Bacteria-Surface Interaction Area

An example result, for monovalent capture, is shown in Figure A3A. Here, for n_{crit} =1, the bacteria-surface interaction area is varied from 500 to 10,000 nm^2, corresponding roughly to interaction diameters of 22-100 nm. The chemico-physical factors contributing to the interaction area are discussed in the main body of this paper. In Figure A3A, the calculated probability for bacterial capture all pass through the origin, the main signature of monovalent capture. The slopes of these predictions, however, are strongly dependent on the interaction area. Therefore, comparing the slope of the predicted bacterial capture probabilities to experimental rate data in the regime of monovalent bacterial capture allows the interaction area to be precisely assessed. Conducting this analysis in what is clearly the monovalent regime allows determination of the interaction area to be decoupled from separate analysis of the numbers of nanoparticles involved in capture.

In Figure 3C of the main paper, for κ^{-1}=4 nm and γ = 22 s^{-1}, monovalent bacterial capture is observed. These experimental data rise linearly (within experimental error) from the origin to an efficiency of unity (corresponding to the transport-limited bacterial capture rate) near about 400 nanoparticles/ um^2 of substrate. In comparing this data to Figure A3A, the key step is to estimate the point where the transport-limited rate caps the ability to experimentally measure high bacterial capture probabilities. The red lines in Figure A3A indicate example probabilities which might become experimentally obscured by transport considerations. Choosing the cut-off too high (B), makes it impossible to fit any of the predicted curves to the data: In Figure A3B, the renormalized calculation, an interaction area of 10,000 nm^2 is too curved as it approaches a probability of unity, and it reaches this limit at a nanoparticle loading of less than 200

$\#/\mu m^2$ while the experimental observations are mostly linear up to 400 nanoparticles/ μm^2. With this choice (B) of transport-limited cut-off, the 5000 nm^2 predictions approach the experimental data; however, the data appear more linear than the predictions. This part of the analysis argues that the choice, B, in Figure A3A is simply too high.

Guessing a lower cut-off (C) produces a more reasonable mapping of capture probability to bacterial capture efficiency (or normalized capture rate.) From this particular choice, which corresponds to the efficiency plot of Figure A3C, the experimental data of Figure 3C most closely match the predictions for $A = 2500$ nm^2, or an interaction radius of about 50 nm. Of course, choosing the transport-limit to be even lower on the main plot (Figure A3A) will reduce the estimated initial interaction area, so this exercise provides an upper limit. The predictions, are, however, clear. The interaction area is not 10,000 nm^2. That figure is far too great. The estimate of 1000 nm^2, corresponding to a contact diameter of 30 nm is likely on the small side.

This exercise in comparing the monovalent capture probabilities to the observed capture rates suggests the initial bacterial-surface interaction area is approximately 2500 nm^2, or in the range 1000-5000 nm^2, an estimated which carries into the main paper for analysis of the number of nanoparticles involved in multivalent capture.
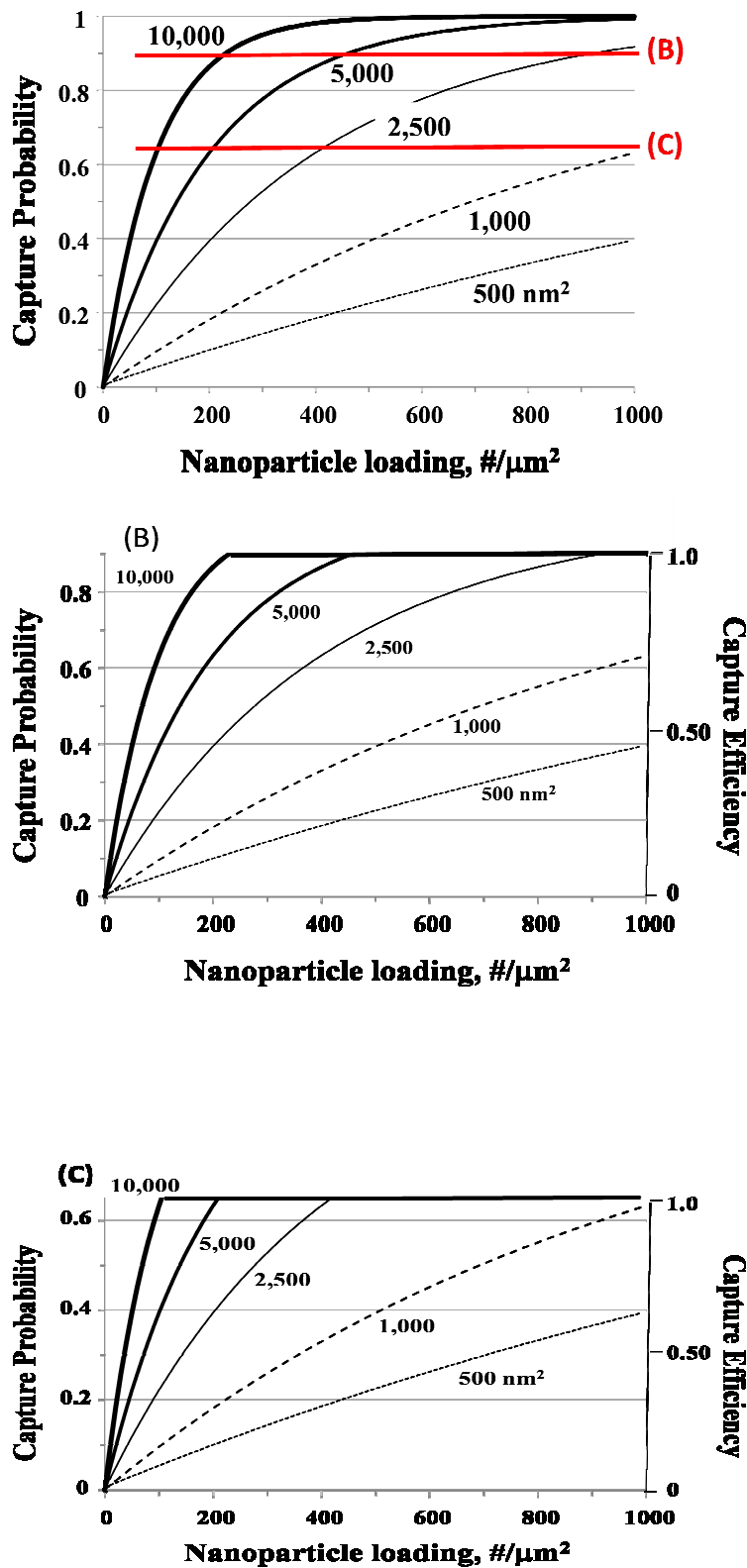
Figure A3. **(A)** Monovalent capture probabilities for different bacterial-surface contact areas. Two arbitrary transport-limited cut offs are indicated, translating to parts B and C of the figure. **(B)** Monovalent capture probabilities and capture efficiencies for a transport –limited ceiling corresponding to 90% capture probability. **(C)** Monovalent capture probabilities and capture efficiencies for a transport –limited ceiling corresponding to 64% capture probability.

References for Supporting Information

(1)   Leveque, M. A. *Ann. Mines* **1928**, *13*, 284.
(2)   Adamczyk, Z.; Siwek, B.; Szyk, L. *J. Colloid Interface Sci.* **1995**, *174*, 130.
(3)   Ko, C. H.; Elimelech, M. *Environ. Sci. Technol.* **2000**, *34*, 3681.
(4)   van Loenhout, M. T. J.; Kooij, E. S.; Wormeester, H.; Poelsema, B. *Colloid Surf. A-Physicochem. Eng. Asp.* **2009**, *342*, 46.
(5)   Duffadar, R.; Kalasin, S.; Davis, J. M.; Santore, M. M. *J. Colloid Interface Sci.* **2009**, *337*, 396.
(6)   Zhang, J.; Srivastava, S.; Duffadar, R.; Davis, J. M.; Rotello, V. M.; Santore, M. M. *Langmuir* **2008**, *24*, 6404.